Scientific paper

Synthesis of CuO by Electrospinning Method for Sensing of Hydrogen and Carbon Monoxide Gases

Abdollah Fallah Shojaei[1]*and Parisa Fallah Komsari[1*]

[1] *Department of Chemistry, Faculty of Science, University of Guilan, P. O. Box, 41335-1914, Rasht, Iran*

** Corresponding author: E-mail: shoja47@yahoo.com, a.f.shojaie@guilan.ac.ir*

Received: 05-01-2021

Abstract

The pure CuO nanofibers were synthesized via the electrospinning method successfully. The calcinated CuO nanofibers were investigated for sensing hydrogen and carbon monoxide gases. Structural properties of the synthesized calcinated nanofibers were studied using Fourier –transform infrared spectroscopy (FTIR), X-ray diffraction (XRD), Energy-dispersive X-ray spectroscopy (EDX), and particle morphology by scanning electron microscopy (SEM). SEM images confirmed string-like structures, nanofibers. The sensor based on the calcinated CuO nanofibers exhibited excellent gas sensing performance at the low operating temperature of 175 °C and the fast response and recovery characteristics at a low concentration. Moreover, good stability, prominent reproducibility, and excellent selectivity are also observed based on the calcinated nanofibers. These results demonstrate the potential application of calcinated CuO nanofibers for sensing hydrogen (10–200 ppm) and carbon monoxide (400–700 ppm) gases.

Keywords: CuO, Carbon Monoxide, Electrospinning, Hydrogen, Calcinated nanofibers

1. Introduction

Metal oxide semiconductor (MOS) gas sensors have gained special focus driven by their diverse applications in air quality detection, inflammable gas inspection, environmental monitoring, healthcare, defense, security, and so on.[1] Semiconducting metal oxides have been extensively used as sensing materials; resistance changes in oxide based semiconductor gas sensors are used to monitor reducing, toxic and inflammable gases, such as NH_3, NO_2, H_2 and CO.[2]

In recent years, huge efforts have been made to develop nanostructured metal oxides with p-type semiconductivity.[3] Copper oxide (CuO) has a narrow band gap (1.2 eV)[4] as a p-type semiconducting oxide is known for being an excellent catalyst of Hydrogen gas.[5] Copper oxide has increasingly attracted interest for both fundamental and practical reasons. It was shown to be an industrially important material that can be widely used in applications such as gas sensors, magnetic storage media, solar energy transformation, semiconductors, and catalysis[6]. A variety of methods such as thermal oxidation,[7] hydrothermal,[8] and electrochemical deposition[9] have been proposed and investigated for the fabrication of low dimensional CuO. Among these methods, electrospinning is one of the most attractive strategies for producing nanofibers of CuO. The electrospinning method involves the following steps: (1) Preparation of sol with suitable inorganic precursor and polymer content and achieving the right rheology for electrospinning, (2) Spinning of the solution to obtain fibers of polymer/inorganic composite, (3) Calcination of the composite fibers to obtain final oxide fibers. It is important; however, to control all of the above three stages to obtain high quality fibers with the desired final properties.[10] It has the merits of simplicity, high efficiency, low cost, and high reproducibility.[11] In the other hand, many studies have reported on H_2 and CO gases sensing. For example, in 1950, Wagner et al. reported the variation of electrical properties when ZnO is exposed to reducing gases.[12] After that, a series of research works about the sensing behavior of MOS to reducing gases were reported by Seiyama, et al. since the 1960s.[13] Up to the present, many kinds of MOS were investigated as hydrogen and carbon monoxide sensing materials, Some of the MOS were studied for measuring hydrogen gas include the following: ZnO which measures a mixture of H_2, CO, CH_4 gases at 300–500 °C,[14] group-III-element-doped ZnO,[15] SnO_x/Pt (Response to 3000 ppm at 250 °C.),[16] Cu/SnO_2 (Response to 435 ppm at 270 °C.),[17] In_2O_3 (Sensitivity values (S) for CO and H_2 (1000 ppm) in air were obtained at 350 °C.),[18] $SrCe_{0.95}Yb_{0.05}O_3$ (The response of hydrogen to 30,000–90000 at 1000 °C.),[19] Cd-doped SnO_2 (Sensitivity to 1000 ppm H_2 and 1000 ppm

CO at 300 °C.),[20] CuO- and ZnO-doped SnO_2 (The response to 200 ppm H_2 and CO at 310 °C.)[21] F-doped SnO_2 (Response to 100 ppm H_2 gas is 2.2 approximately.)[22] Co-doped SnO_2 (Response to 100 ppm of H_2 gas at 330 °C),[23] Pd-doped SnO_2 (gas sensing to 100 ppm H_2 and 100 ppm CO at 385 °C.),[24] SnO_2 (Response to 10000 ppm H_2 gas at 150 °C.)[25] CuO (The sensitivity of the sensor in response to 100 ppm H_2 at 300 °C is ~2.5.)[26] SnO_2 (Response to 1000 ppm H_2 at 400 °C.),[27] TiO_2 (The sensitivity of the sensor in response to 1000 ppm H_2 at 300 °C is ~3.75.)[28]

And some of MOS were studied to measure CO gas are: Cu-doped ZnO (Its Sensitivity to carbon monoxide at 350 °C is ~ 3.)[29], SnO_2 (The sensitivity of the sensor in response to 1000 ppm carbon monoxide at 200 °C is 3.5.)[30] SnO_2 doped with Pd and Pt (CO sensing at 450 °C),[31] Nb–TiO_2 (Response to CO (1000 ppm) at 550–950 °C.),[32] In_2O_3/ SnO_2 (The selectivity to CO gas at 200 °C.),[33] CuO (Sensitivity to CO gas at 300 °C.),[34] ZnO-doped SnO_2(The response to carbon monoxide at 300 °C.)[35] ZnO_2 (measured CO concentrations ranging from 100 ppm to 1000 ppm.).[36]

In this paper, we reported a simple and facile approach to fabricate high quality calcinated CuO nanofibers by electrospinning and their H_2 and CO sensing characteristics are investigated. The study focuses on the design of CO and H_2 sensors with minimum interference with other Volatile organic compounds. The high response, quick response, and recovery, and good selectivity are observed in our investigation, which indicates the potential application of calcinated CuO nanofibers for the fabrication of high performance H_2 and CO sensors.

1. 1. Gas Sensing Performances

The gas sensing properties of unloaded and loaded-MOS nanoparticles sensing films are characterized in terms of response, response time, and recovery time as a function of operating temperature, gas concentration, and metal loading. The resistance of the p-type metal oxide surface increases because generated electrons recombine with holes, decreasing the hole concentration. The response for p-type semiconducting oxide to reducing gas (S^p) becomes:

$$S^p = \frac{Rg}{Ra} \quad (1)$$

where R_g and R_a are the electrical resistances of the sensors measured in the presence of reducing gas and pure dry air, respectively. The response time, T_{res} is defined as the time required reaching 90% of the steady response signal. The recovery times, T_{rec} denotes the time needed to recover 90% of the original baseline resistance. Moreover, the selectivity defined as the response ratio of target gas to that of another gas is used to assess the relative performance of Semiconducting metal oxides (MOXs) sensors towards different gases.[37] In this paper the sensitivity (S) was defined as $S = R_g/R_a$.

A possible sensing mechanism is described as follows to discover the gas sensing reaction process of the CuO sensor against H_2 and CO gases and illustrate the enhanced H_2 and CO sensing properties of the calcinated CuO nanofibers.

As described in Figure 1, under an air atmosphere the oxygen molecules can get adsorbed on the surface of

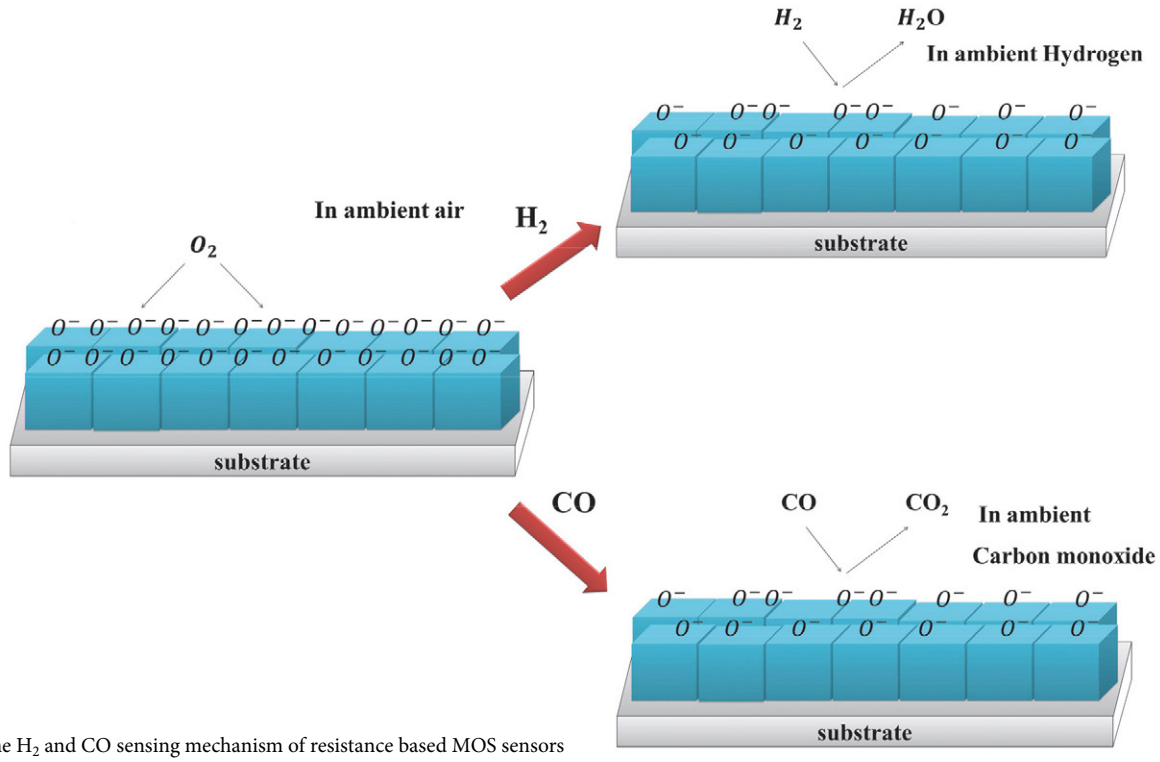

Figure 1. The H_2 and CO sensing mechanism of resistance based MOS sensors

the semiconductor and extracts electrons from the conduction band to form oxygen ions.[38] The adsorption of oxygen forms ionic species such as O^{2-}, O^{-} and O^{2-}, which acquire electrons from the conduction band. The reaction kinetics may be explained by the following reactions: [39,40]

$$O_2(g) \leftrightarrow O_2(ad) \quad (2)$$

$$O_2(ad) + e^- \leftrightarrow O_2^-(ad) \quad (3)$$

$$O_2^- + e^- \leftrightarrow 2O^- \quad (4)$$

$$O^- + e^- \leftrightarrow O^{2-} \quad (5)$$

H_2 and CO sensing mechanisms of the MOS can be explained from the following reaction paths:[41]

$$H_2(g) + O^-(ad) \rightarrow H_2O + e^- \quad (6)$$

$$H_2(g) + O^{2-}(ad) \rightarrow H_2O + 2e^- \quad (7)$$

And :[42]

$$2CO + O_2^- \rightarrow 2CO_2 + e^- \quad (8)$$

$$CO + O^- \rightarrow CO_2 + e^- \quad (9)$$

$$CO + O^{2-} \rightarrow CO_2 + 2e^- \quad (10)$$

2. Experimental

2. 1. Materials and Methods

Ethanol (>99%), N, N-dimethyl formamide (>99%, DMF), $CuCl_2$ $6H_2O$ were used and purchased from Merck Company. Poly vinyl pyrrolidone (PVP, Mw = 1,300,000) and poly vinyl alcohol (PVA, Mw = 31,000–50,000) were obtained from Sigma Aldrich and also distilled water was used. All chemicals were analytical grade and used as received without any further purification.

The Fourier transforms infrared spectroscopy (FT–IR) of the calcinated CuO nanofibers were recorded on Thermo Nicolet Avatar spectrophotometer in the range of 500–4000 cm^{-1} using KBr pellets. The X-ray diffraction (XRD) technique (PHILIPS XRD diffractometer using Cu K_α (K_α = 1.540 Å and 2θ = 10–90 radiation as X-ray source) was used to verify the structure of the calcinated CuO nanofibers. Scanning electron microscopy (SEM) calcinated nanofibers images were performed on an LEO 1450 VP (Germany) instrument, Energy Dispersive X-ray spectroscopy (EDX) was attained on a TESCAN S8000 microscope, Atomic Absorption Spectrometer (AAS) of calcinated nanofibers were performed on an Agilent 240 AA instrument and Spin coating Device (Institute for Research and Technology Development of Modern Industry, Made in Iran) was a used to deposit uniform thin films onto flat glass.

2. 2. Synthesis of CuO nanofibers

The electrospinning process was employed for CuO nanofibers synthesis. A mixed solution of polyvinyl alcohol (PVA, Mw: 31,000–50,000) and Copper (II) chloride ($CuCl_2$ $6H_2O$) was used for electrospinning. In the typical experimental procedure, a PVA solution (10 wt %) was first prepared by dissolving PVA powder in distilled water and stirred for 5 h at 60 °C. A 20 wt% $CuCl_2$ solution and PVP powder was added to this solution. After stirring for 12 h, this mixed solution was introduced in a 20 mL syringe equipped with a metal needle tip in a controlled electrospinning setup. The parameters for electrospinning were selected as; applied voltage: 20 kV, feeding rate of the solution: 0.2 mL/h, distance between glass substrate attached to the copper sheet, and the tip of the needle: 10 cm. Finally, the fibers were peeled off from the collector with tweezers and placed in a crucible. The conversion of copper dichloride to CuO and the removal of organic constituents PVP and PVA in the as-spun nanofibers were achieved by calcining at 400 °C for 2 h in air.

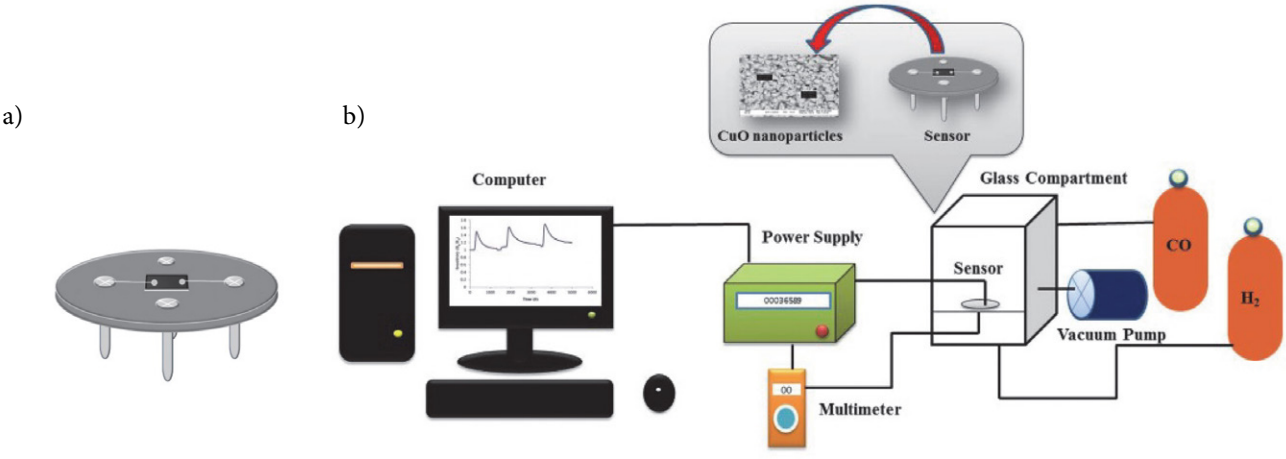

Figure 2. Schematic image of (a) sensor kit, and (b) the gas-sensing analysis system.

2. 3. Gas Identification System

Gas sensors were manufactured by Spin coating technique with planar glass substrates. Fig.2 (a) shows the schematic of the sensor. The as-prepared calcinated CuO nanofibers were blended with deionized water in a weight ratio of 100: 25 to form a paste. Then the paste was subsequently screen-printed onto the planar glass substrate to form a sensing film with a thickness of about 60 μm, the manufactured sensor was dried in air at room temperature to volatilize the water solvent and last aged in an aging test chamber for 24 h and after a Ni–Cr heating wire was inserted in the underneath to form a side-heated gas sensor. The efficiency of the gas sensors was determined in a gas testing chamber. Detail of the measurement setup can be observed in the schematic diagram is presented in Fig.2 (b). Electrical linkages to the gas sensors were achieved by physically connecting needle probes to the Pt electrodes of the sensors. A PC 510a (japan) multimeter was applied for measuring the changes of sensor resistance over time and a computer was used for logging data from the multimeter. At first, the responses of the sensors were measured in the presence of 200 ppm H_2 gas and 700 ppm CO gas in the ambient air where the temperatures were modified in the range 25–175 °C in order to ascertain their optimum operating temperature. The sensors were pre-heated at different operating temperatures for about 45 min. When the resistances of all the sensors were stable, saturated target gas was injected into the test chamber (20 L in volume) by a micro injector through a rubber plug. After its resistance value reached a new constant value, the test chamber was opened to recover. The sensor resistance and sensitivity were collected and analyzed by the system. And the environmental temperature, relative humidity, and working temperature were recorded.

3. Results and Discussion

3. 1. Identification of Sensor Structure

The X-ray diffraction pattern of the CuO nanofibers at 400 °C for 2h (calcinated CuO nanofibers) is shown in Fig. 3. The CuO peaks appear at diffraction angles of 32/53°, 35/55°, 38/75°, 48/75°, 51/40°, 58/35°, 61/57°, 66/28°, 68/14°, 73/01°, 75/28° corresponding to reflection from (1 1 0), (0 0 2), (1 1 1), (-2 0 2), (0 2 0), (2 0 2), (-1 1 3), (-3 1 1), (2 2 0), (3 1 1), and (-2 2 2) planes, respectively. The strongest diffraction pattern viewed at 2θ = 35/55 suggests that the CuO grows with a preferential orientation of (0 0 2) on the glass plate and illustrates the formation of the single-phase of monoclinic CuO. It was also viewed that the obtained XRD spectra are in very good agreement with reported 2θ values in JCPDS card no 48–1548.[43] Also, the average CuO particle size (D) was calculated using the Scherrer equation (11) is resulted 60 nm in one dimension, where D is the nanocrystal size; K is the shape factor, usually taken as 0.89 for ceramic materials (K has a typical value of about 0.9); λ is the wavelength of radiation in nanometer ($\lambda_{CuK\alpha}$ = 0.15405 nm); θ is the diffracted angle of the peak; β is the full width at half maximum of the peak in radians.[44]

$$D = \frac{K\lambda}{\beta \cos\theta} \tag{11}$$

Fig. 4(a) shows the SEM image of the nanofibers, this precursor at room temperature it has an average diameter of about 80 nanometers and several tens of micrometers in length. After calcination for 2h at 400 °C, the length of the product, as shown in Fig. 4(b), is shorter than that of the precursor. The average diameter of calcinated CuO nanofibers at 400 ° C is approximately 70 nm.

The FT-IR absorption peaks were performed to confirm the presence of characteristic vibrational peaks of calcinated CuO nanofibers. The FT-IR spectrum of the calcinated CuO nanofibers is presented in Fig. 5. The observed strong peaks at around 529, 585, and 672 cm^{-1} are attributed to the stretching from Cu-O along (-2 0 2) direction.[45] The absorption peak around 1100 cm^{-1} may be attributed to –OH bending vibrations of Cu-OH.[46] The transmittance peak that appeared at around 1377 cm^{-1} may be ascribed due to the presence of CO_2, which is usually adsorbed from the air on the surface of sample materials during KBr pelletization.[47] The corresponding CH_2 bend placed at around 1460 cm^{-1}.[48] The weak band

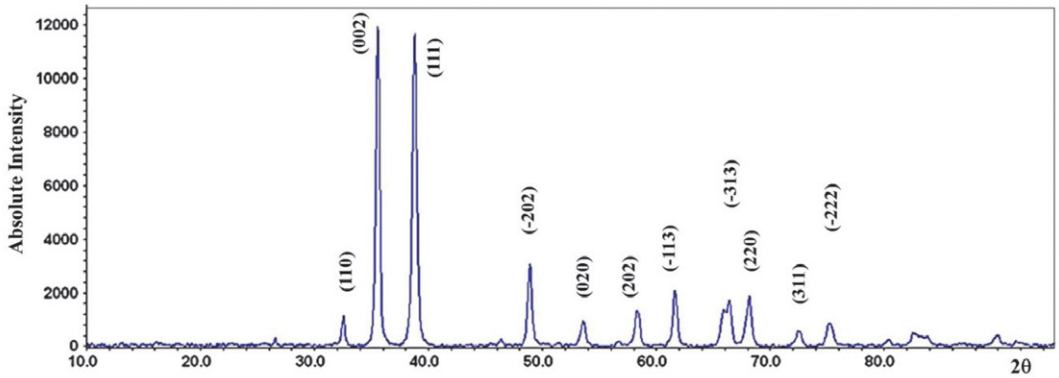

Figure 3. X-ray diffraction pattern of CuO nanofibers calcined at 400 °C for 2 h (calcinated CuO nanofibers).

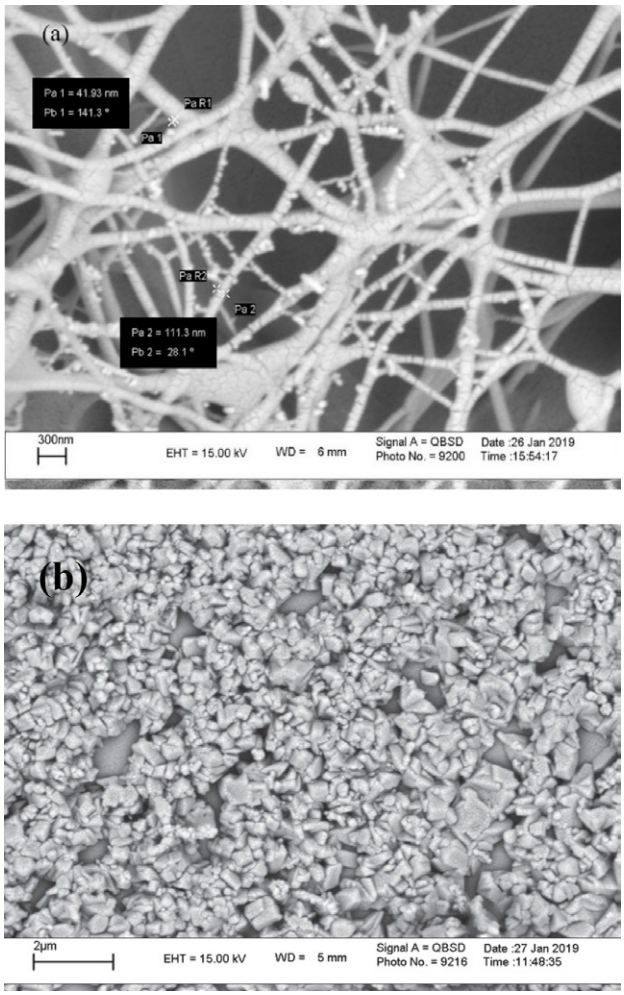

Figure 4. SEM image of (a) CuO nanofibers (b) CuO nanofibers calcinated at 400 °C for 2 h.

at 1639.76 cm^{-1} may be attributed to the bending vibration modes of O–H groups of these adsorbed H_2O molecules.[49] Further, three small bands at 2862.62, 2928.94, and 2959.97 cm^{-1} may be ascribed to the asymmetric and symmetric vibrational modes of the O–H bond of the H_2O molecules physisorbed on the surface of the CuO.[50] An intense broadband appeared in the 3400–3800 cm^{-1} region that was attributed to the O–H stretching vibration of surface hydroxyl groups of adsorbed water molecules, [51] which arises because nanocrystalline materials having a high surface-to-volume ratio absorbs high moisture.

The EDX spectrum of the calcinated CuO nanofibers is reported in Fig. 6. Only Cu and O signals have been detected, indicating that the calcinated nanofibers were only built up of Cu and O. Weight percent of Cu was found to be 68.42 and that of O was 31.58. Thus the atomic ratio of Cu and O was 1:1. And 2.8 Peak is for the gold metal due to the preparation of the sample for EDX analysis.

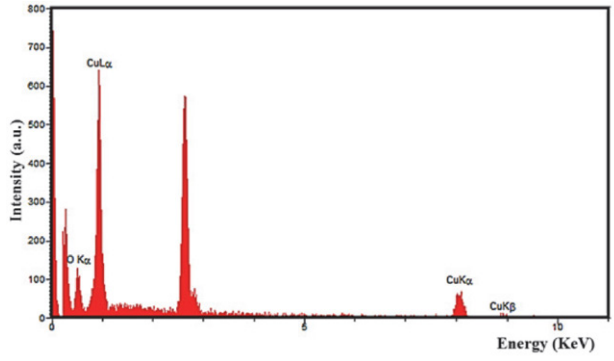

Figure 6. EDX spectra of calcinated CuO nanofibers.

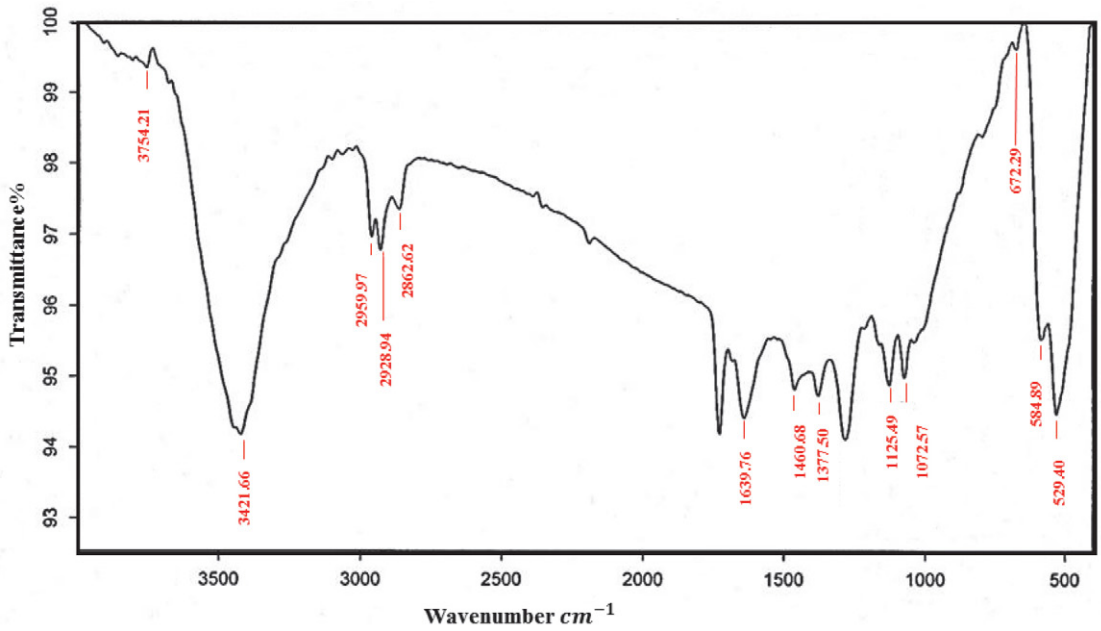

Figure 5. FTIR spectra of calcinated CuO nanofibers.

3. 2. Gas Sensing Characteristics

To determine the optimum operating temperature, the responses of the calcinated CuO nanofibers gas sensor to 200 ppm H_2 and 700 ppm CO were measured continually at different operating temperatures. Fig. 7 shows the responses as a function of operating temperature from 25 to 300 °C. For each gas, the response is measured to increase rapidly with increasing operating temperature and arrive at the maximum and then decreases with a further rise of the operating temperature. The optimum operating temperatures of the calcinated CuO nanofibers are suggested at 175 °C for both H_2 and CO gases with response values of 5.43 and 9.14, respectively.

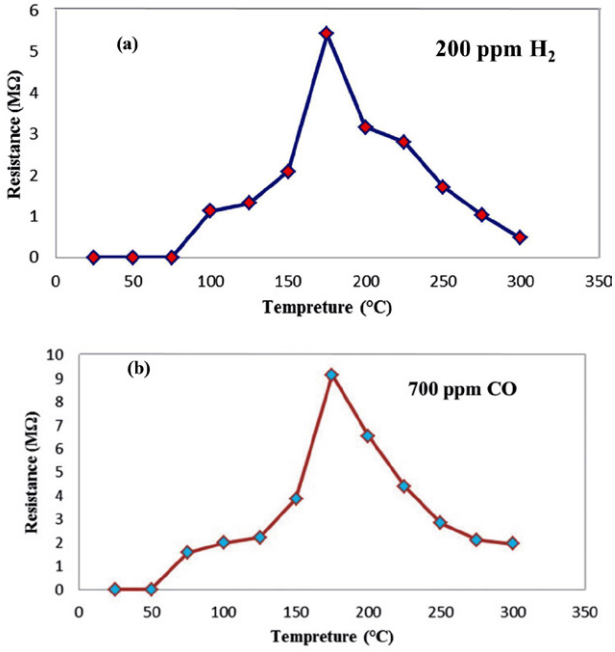

Figure 7. Responses of the calcinated CuO nanofibers sensors to (a) 200 ppm of H_2 and (b) 700 ppm of CO at different operating temperatures.

It is well known that response and recovery characteristics are important for evaluating the performances of semiconductor oxide sensors. The gas sensing transients of the calcinated CuO nanofibers sensor upon exposure to H_2 (200 ppm) and CO (700 ppm) are shown in Fig. 8. The gas responses and response speeds differed significantly according to the sensor temperature and type of gas. The times to reach 90% variation in resistance upon exposure to gas and air were defined as the 90% response time (τ_{res}) and the 90% recovery time (τ_{recov}), respectively. Most of the τ_{res} values were very short, indicating that both in the diffusion of analyte gas and the oxidation reaction between analyte gas and negatively charged chemisorbed oxygen occur very rapidly. Fast gas diffusion in the present study was attributed to the large surface area of calcinated nanofibers. fig. 8 (a) shows the response time of the designed sensors for hydrogen and carbon monoxide gas was 39 s and 53 s at 175 °C, respectively. The recovery time for hydrogen and carbon monoxide gas was 94 s and 67 s at175 °C, respectively (fig.8 (b)).

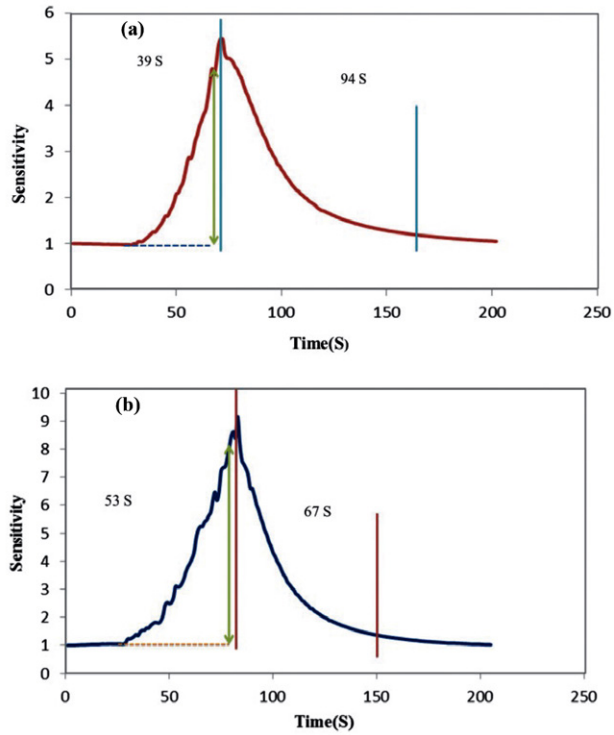

Figure 8. A single-cycle response–recovery characteristic curves of calcinated CuO nanofibers to (a) 200 ppm H_2 and (b) 700ppm CO at 175° C.

Selectivity of H_2 and CO sensors couldn't be measured at the same time to justify the detection of one gas; there for Sensitivity of gases was measured separately during the experiment. To investigate the stability and repeatability of the calcinated CuO nanofibers sensor, it was sequentially exposed to different concentrations of H_2 gas Separately (10, 25, 50,100, and 200 ppm) as shown in Figure 9 and shows the best response with more drastic resistance in concentration 200 ppm of H_2. also Fig. 10 (a-d) presents three reversible cycles response curve in the concentration range of 400–700 ppm of the that confirmed the calcinated CuO nanofibers had excellent stability and reversibility when alternately exposed to air and CO gas and it was found that calcinated CuO nanofibers showed extremely excellent CO sensing performances at concentration 700 ppm with the highest sensor response and the highest selectivity compared to the other CO concentrations. As shown in Figures 9 and 10, the sensor response increases rapidly when exposed to a certain concentration of H_2 and CO and decreases dramatically when exposed to air for recovery. Meanwhile, the gas response of the sensor always returns to its initial value during the continuous test period, implying a very satisfying reproducibility of the prepared sensor.

The concentration dependence of calcinated CuO nanofibers was investigated in the concentration range of 10–200 ppm of H_2 and the concentration range of 400–700 ppm CO the plots of the gas response against gas concentration

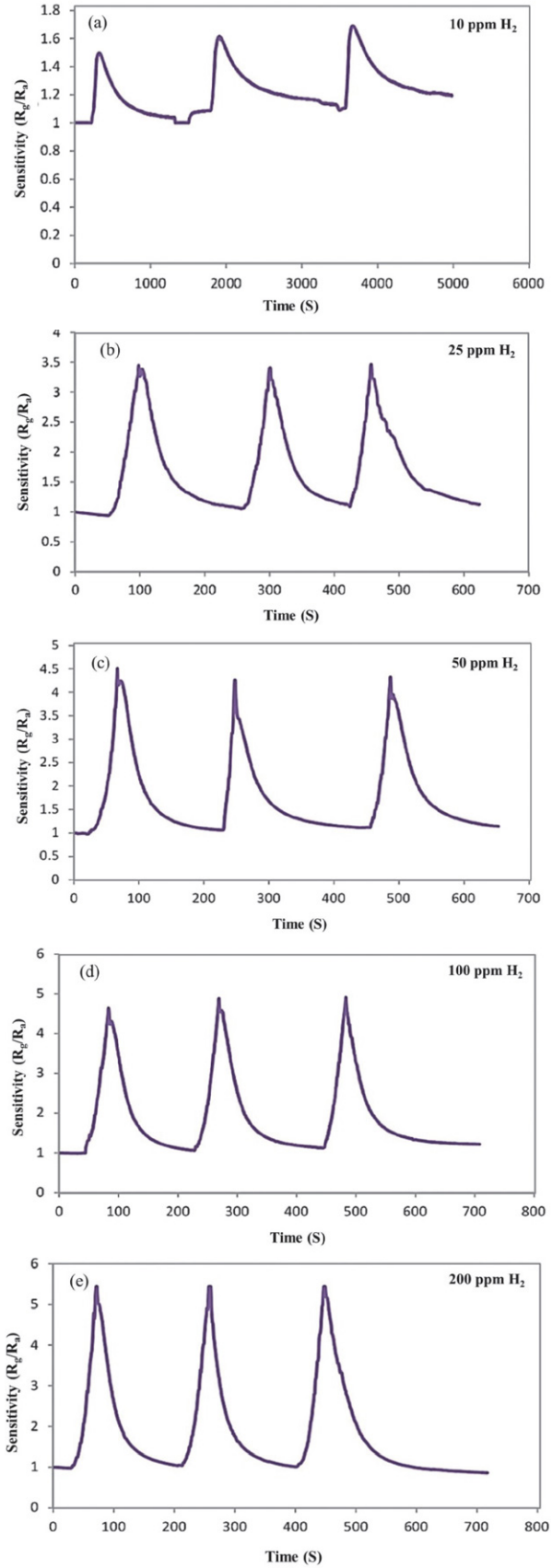

Figure 9. Reproducibility of the calcinated CuO nanofibers sensor on successive exposure (3 cycles) to (a) 10 ppm (b) 25 ppm (c) 50 ppm (d) 100 ppm (e) 200 ppm of H_2 at 175°C.

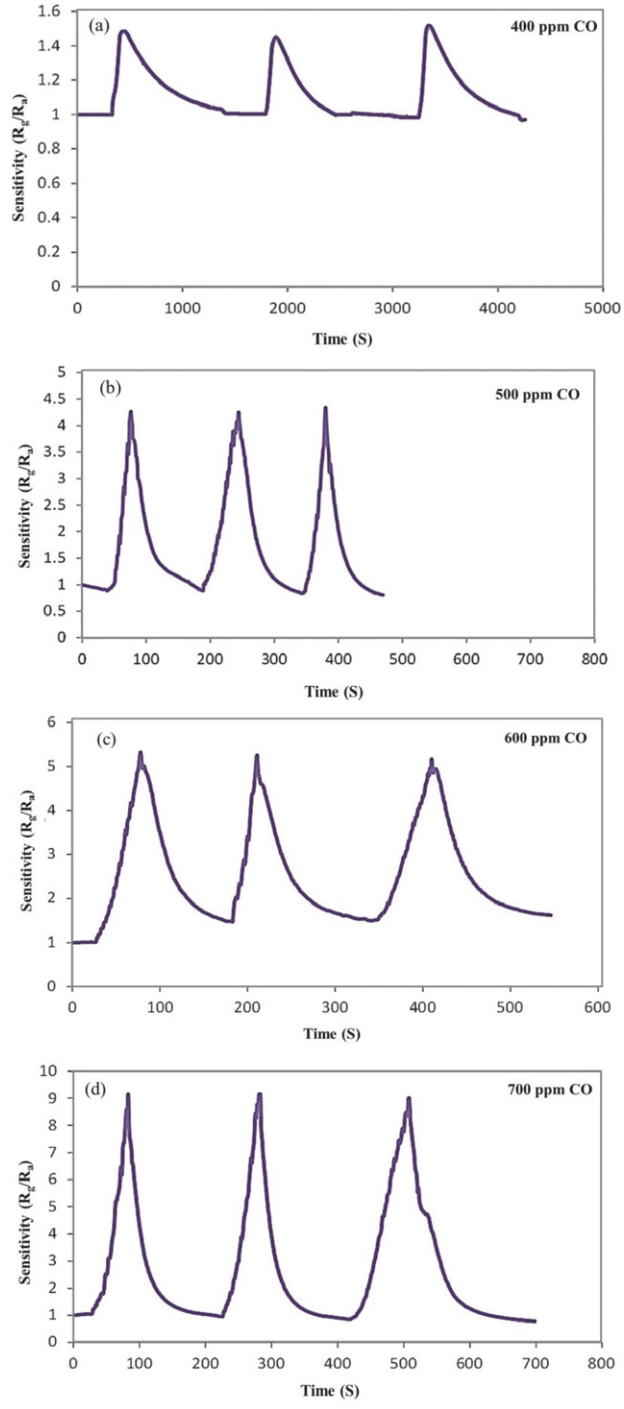

Figure 10. Reproducibility of the calcinated CuO nanofibers sensor on successive exposure (3 cycles) to (a) 400 ppm (b) 500 ppm (c) 600 ppm (d) 700 ppm of CO at 175°C.

are shown in Figure 11(a–b). As shown in Figure 11 (a), as the H_2 concentration increases to 50 ppm, the gas response increases linearly, and at 100 and 200 ppm the graph's slope decreases but the response is still rapid. This indicates that the sensor is not saturated. Thus, the calcinated CuO nanofibers sensor has a relatively linear relation to detecting H_2 at concentrations 10, 25 and 50 ppm at the log scale, and

also the calcinated CuO nanofibers sensor has a linear relationship to detect CO at the log scale. Thus calcinated CuO nanofibers sensor is favorable to detect H_2 and CO.

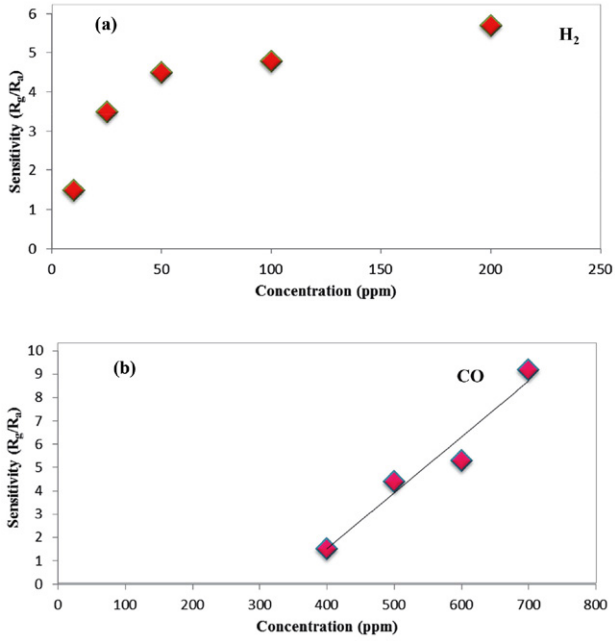

Figure 11: Responses of the calcinated CuO nanofibers sensor to different concentrations of (a) H_2 and (b) CO at 175 °C.

The gas sensing selectivity is another very important parameter to appraise the sensing ability of metal oxide semiconductor materials. Fig. 12 describes the histogram of the gas response of the calcinated CuO nanofibers sensor to 10 ppm of various gases, including n-hexane, methanol, ethanol, acetaldehyde, formaldehyde, and hydrogen at 175 °C. To demonstrate the sensor's high sensitivity to hydrogen gas than various gases, 10 ppm of various gases including: n-hexane, methanol, ethanol, acetaldehyde, and formaldehyde) are injected separately to test sensor sensitivity. And the sensitivity(S) results are presented in the form of a bar graph in Figure 12.

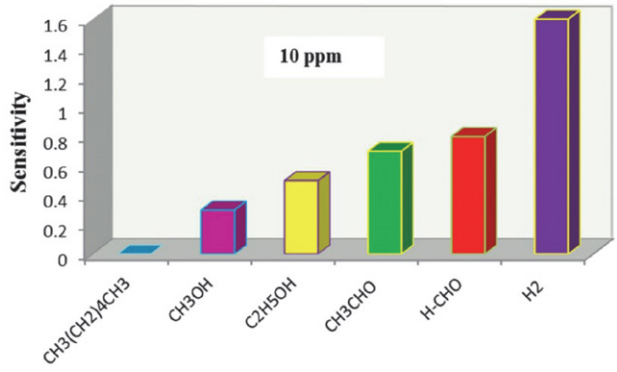

Figure 12. The selectivity of the calcinated CuO nanofibers sensor on successive exposure to 10 ppm of various gases at 175°C.

This sensor shows an obvious hydrogen sensing response than other potential interface gases. Therefore, we believe that the calcinated CuO nanofibers gas sensor has an excellent selectivity to10 ppm of H_2.

The comparison of calcinated CuO nanofibers sensor performance and recently reported data in the literature for hydrogen and carbon monoxide sensing applications are shown in Table 1. The sensitivity of calcinated CuO nanofibers at low temperature (175 °C) to 200 ppm of hydrogen gases with a response time of 39 s and 700 ppm of carbon monoxide with a response time of 53 s is 5.5 and 9.3, respectively. Low detection limit and low temperature, high sensitivity have shown promising results compared to other literature Table 1.

4. Conclusion

In summary, pure calcinated CuO nanofibers are synthesized via a simple electrospinning method and characterized by FT-IR, XRD, SEM, and EDX. The sensor exhibited the highest sensitivity (response: Rg/R_a = 5.43) to 200 ppm hydrogen and (response: Rg/R_a = 9.14) to 700 ppm Carbon monoxide at 175 °C. Short response and re-

Table 1. Comparison of calcinated CuO nanofibers sensors parameters and previous researches.

Sensing material	gas	Detection limit (ppm)	Operating temperature (°C)	Sensitivity (R_g/R_a)	Synthesis method	Response time	Ref.
CuO	H_2	60000	300–800	3.72	Thermal oxidation	5 (min)	52
CuO	H_2	1000	300	3	Sputtering	10 (S)	53
30Pd/CuO	H_2	1000	200	4.5	Hydrothermal	10(min)	54
CuO	H_2	1000	200	0.4	Anodization	~9(min)	55
Pd Doped TiO_2 – CuO	H_2	3000	150	–	Sol-gel	–	56
CuO	H_2	200	175	5.5	Electrospinning	39 (S)	This work
CuO	CO	1000	300	1.6	Sputtering	–	53
CuO–ZnO	CO	800	500	–	Thermal evaporation	3.2 (min)	57
CuO-Cu*x*Fe_3–*x*O_4	CO	500	400	1.9	Sputtering	21(min)	58
0.4% Pt/ZnO–CuO	CO	1000	RT	2.64	Thermal	81(S)	59
CuO	CO	700	175	9.2	Electrospinning	53 (S)	This work

covery times and excellent selectivity are indicated based on calcinated CuO nanofibers that can be fabricated more quickly and at a lower cost. The simple method reported here can be used for further improving gas sensor performance such as enhancing the selectivity of the gas sensors to different test gases.

Acknowledgments

This study was supported by the Science and Research Branch, University of Guilan.

Conflict of Interest

The authors declare that there are no conflicts of interest regarding the publication of this manuscript.

5. References

1. L. Li, C. Guo, S. Li, L. Wang, Q. Dong, W. Li, *Sens. Actuators, B*. **2010**, *150*, 806–810. **DOI:**10.1016/j.snb.2010.07.022
2. C. C. Hsiao, L. S. Luo, *Sensors*, **2014**, *14*, 12219–12232. **DOI:**10.3390/s140712219
3. J. Jayaprakash, N. Srinivasan, P. Chandrasekaran, & E. K. Girija, *Spectrochim. Acta, Part A*. **2015**, *136*, 1803–1806. **DOI:**10.1016/j.saa.2014.10.087
4. H. Xiang, Y. Long, X. Yu, X. Zhang, N. Zhao, & J. Xu, *CrystEngComm*. **2011,** *13*, 4856–4860. **DOI:**10.1039/c0ce00980f
5. N. D. Hoa, S. Y. An, N. D. Dung, N. V. Quy, D. Kim, *Sens. Actuators, B*. **2010**, *146*, 239–244. **DOI:**10.1016/j.snb.2010.02.045
6. H. Guan, C. Shao, B. Chen, J. Gong, & X. Yang, *Inorg. Chem. Commun.* **2003,** *6*, 1409–1411. **DOI:**10.1016/j.inoche.2003.08.021
7. D. T. T. Le, N. Van Duy, N. D. Hoa, N. Van Hieu, *Phys. E (Amsterdam, Neth.)*. **2014**, *58*, 16–23. **DOI:**10.1016/j.physe.2013.11.013
8. M. A. Dar, Y. S. Kim, W. B. Kim, J. M. Sohn, H. S. Shin, *Appl. Surf. Sci.* **2008**, *254*, 7477–7481. **DOI:**10.1016/j.apsusc.2008.06.004
9. L. Chen, S. Shet, H. Tang, H. Wang, T. Deutsch, Y. Yan, J. Turner, M. Al-Jassim, *J. Mater. Chem.* **2010**, *20*, 6962–6967. **DOI:**10.1039/c0jm01228a
10. N. V. Dung, D. T. T. Le, N. D. Trung, H. N. Dung, N. M. Hung, N. V. Duy, & N. V. Hieu, *J. Nanosci. Nanotechnol.* **2016** *16*, 7910–7918. **DOI:**10.1166/jnn.2016.12747
11. X. Shi, W. Zhou, D. Ma, Q. Ma, D. Bridges, Y. Ma, A. Hu, *J. Nanomater.* **2015**, *16*, 122. **DOI:**10.1155/2015/140716
12. C. Wagner, *J. Chem. Phys.* **1950**, *18*, 69–71. **DOI:**10.1063/1.1747459
13. T. Seiyama, A. Kato, K. Fujiishi, M. Nagatani, *Anal. Chem.* **1962**, *34*, 1502–1503. **DOI:**10.1021/ac60191a001
14. B. Bott, T. A. Jones, B. Mann, *Sens. Actuators*. **1984**, *5*, 65–73. **DOI:**10.1016/0250-6874(84)87007-9
15. H. Nanto, T. Minami, S. Takata, *J. Appl. Phys.* **1986**, *60*, 482–484. **DOI:**10.1063/1.337435
16. W. K. Choi, S. K. Song, J. S. Cho, Y. S. Yoon, D. Choi, H. J. Jung, S. K. Koh, *Sens. Actuators, B*. **1997**, *40*, 21–27. **DOI:**10.1016/S0925-4005(97)80194-3
17. A. Galdikas, V. Jasutis, S. Kačiulis, G. Mattogno, A. Mironas, V. Olevano, D. Senulienė A. Šetkus, *Sens. Actuators, B*. **1997**, *43*, 140–146. **DOI:**10.1016/S0925-4005(97)00206-2
18. W. Y. Chung, G. Sakai, K. Shimano, N. Miura, D. D. Lee, N. Yamazoe, *Sens. Actuators, B*. **1998**, *46*,139–145. **DOI:**10.1016/S0925-4005(98)00100-2
19. I. Kosacki, H. U. Anderson, *Sens. Actuators, B*. **1998**, *48*, 263–269. **DOI:**10.1016/S0925-4005(98)00055-0
20. Z. Tianshu, P. Hing, Y. Li, Z. Jiancheng, *Sens. Actuators, B*. **1999**, *60*, 208–215. **DOI:**10.1016/S0925-4005(99)00272-5
21. J. H. Yu, G. M. Choi, *Sens. Actuators, B*. **2001**, *75*, 56–61. **DOI:**10.1016/S0925-4005(00)00742-5
22. C. H. Han, S. D. Han, I. Singh, T. Toupance, *Sens. Actuators, B*. **2005**, *109*, 264–269. **DOI:**10.1016/j.snb.2004.12.115
23. L. Liu, C. Guo, S. Li, L. Wang, Q. Dong, W. Li, *Sens. Actuators, B*. **2010**, *150*, 806–810. **DOI:**10.1016/j.snb.2010.07.022
24. J. K. Choi, I. S. Hwang, S. J. Kim, J. S. Park, S. S. Park, U. Jeong, Y. C. Kang, J. H. Lee, *Sens. Actuators, B*. **2010**,*150*, 191–199. **DOI:**10.1016/j.snb.2010.07.013
25. R. Ab Kadir, Z. Li, A. Z. Sadek, R. Abdul Rani, A. S. Zoolfakar, M. R. Field, J. Z. Ou, A. F. Chrimes, K. Kalantar-Zadeh, *J. Phys. Chem. C*. **2014**, *118*, 3129–3139. **DOI:**10.1021/jp411552z
26. O. Lupan, V. Postica, N. Ababii, M. Hoppe, V. Cretu, I. Tiginyanu, V. Sontea, Th. Pauporté, B. Viana, R. Adelung, *Microelectron. Engin.* **2016**, *164*, 63–70. **DOI:**10.1016/j.mee.2016.07.008
27. N. Xue, Q. Zhang, S. Zhang, P. Zong, F. Yang, *Sensors*, **2017**, *17*, 2351. **DOI:**10.3390/s17102351
28. S. A. Mohd Chachuli, M. N. Hamidon, M. S. Mamat, M. Ertugrul, N. H. Abdullah, *Sensors*, **2018**, *18*, 2483. **DOI:**10.3390/s18082483
29. H. Gong, J. Q. Hu, J. H. Wang, C. H. Ong, F. R. Zhu, *Sens. Actuators, B*. **2006**, *115*, 247–251. **DOI:**10.1016/j.snb.2005.09.008
30. A. Salehi, *Sens. Actuators, B*. **2003**, *96*, 88–93. **DOI:**10.1016/S0925-4005(03)00490-8
31. P. Menini, F. Parret, M. Guerrero, K. Soulantica, L. Erades, A. Maisonnat, B. Chaudret, *Sens. Actuators, B*. **2004**, *103*, 111–114. **DOI:**10.1016/j.snb.2004.04.103
32. T. Anukunprasert, C. Saiwan, E. Traversa, *Sci. Technol. Adv. Mater*. **2005**, *6*, 359–363. **DOI:**10.1016/j.stam.2005.02.020
33. I. J. Kim, S. D. Han, C. H. Han, J. Gwak, H. D. Lee, J. S. Wang, *Sensors*, **2006**, *6*, 526–535. **DOI:**10.3390/s6050526
34. S. Steinhauer, E. Brunet, T. Maier, G. C. Mutinati, A. Köck, O. Freudenberg, C. Gspan, W. Grogger, A. Neuhold, R. Resel, *Sens. Actuators, B*. **2013**, *187*, 50–57. **DOI:**10.1016/j.snb.2012.09.034
35. E. Nikan, A. A. Khodadadi, Y. Mortazavi, *Sens. Actuators, B*. **2013**, *184*, 196–204. **DOI:**10.1016/j.snb.2013.04.089
36. C. C. Hsiao, L. S. Luo, *Sensors*, **2014**, *14*, 12219–12232. **DOI:**10.3390/s140712219
37. T. Samerjai, N. Tamaekong, K. Wetchakun, V. Kruefu, C. Liewhiran, C. Siriwong, A. Wisitsoraat, S. Phanichphat, *Sens.*

Actuators, B. **2012**, *171*, 43–61. **DOI:**10.1016/j.snb.2012.05.052
38. H. Gu, Z. Wang, Y. Hu, *Sensors*, **2012**, *12*, 5517–5550. **DOI:**10.3390/s120505517
39. S. Phanichphant, C. Liewhiran, K. Wetchakun, A. Wisitsoraat, A. Tuantranont, *Sensors*, **2011**, *11*, 472–84. **DOI:**10.3390/s110100472
40. L. F. Dong, Z. L. Cui, Z. K. Zhang, *Nanostruct. Mater.* **1997**, *8*, 815–823. **DOI:**10.1016/S0965-9773(98)00005-1
41. C. Wongchoosuk, A. Wisitsoraat, D. Phokharatkul, A. Tuantranount, T. Kerdcharoen, *Sensors*, **2010**, *10*, 7705–15. **DOI:**10.3390/s100807705
42. C. C. Hsiao, L. S. Luo, *Sensors*, **2014**, *14*, 12219–12232. **DOI:**10.3390/s140712219
43. Y. Zou, Y. Li, X. Lian, D. An, *Research of Materials Science*, **2014**, *3*, 44–51.
44. U. Holzwarth, & N. Gibson, Nat. Nanotechnol. **2011,** *6*, 534–534. **DOI:**10.1038/nnano.2011.145
45. M. A. Das, S. H. Nam, Y. S. Kim, W. B. Kim, *J. Solid State Electrochem.* **2010**, *14*, 1719–1726. **DOI:**10.1007/s10008-010-1022-z
46. D. P. Dubal, G. S. Gund, C.D. Lokhande, R. Holze, *Mater. Res. Bull.* **2013**, *48*, 923–928. **DOI:**10.1016/j.materresbull.2012.11.081
47. S. Sundar, G. Venkatachalam, S. J. Kwon, *Nanomaterials*, **2018**, *8*, 823. **DOI:**10.3390/nano8100823
48. N. Can, *Mater. Chem. Phys*, **2018**, *213*, 6–13. **DOI:**10.1016/j.matchemphys.2018.03.069
49. A. Nezamzadeh-Ejhieh, H. Zabihi-Mobarakeh, *J. Ind. Eng. Chem.* **2014**, *20*, 1421–1431. **DOI:**10.1016/j.jiec.2013.07.027
50. P. K. Raul, S. Senapati, A. K. Sahoo, I. M. Umlong, R. R. Devi, A. J. Thakur, V. Veer, *RSC Adv.* **2014**, 4, 40580–40587. **DOI:**10.1039/C4RA04619F
51. M. Halder, M. M. Islam, Z. Ansari, S. Ahammed, K. Sen, S. K. M. Islam, *ACS Sustain. Chem. Eng.* **2017**, *5*, 648–657. **DOI:**10.1021/acssuschemeng.6b02013
52. N. D. Hoa, S.Y. An, N. Q. Dung, N. Van Quy, & D. Kim, *Sens. Actuators, B.* **2010,** *146*, 239–244. **DOI:**10.1016/j.snb.2010.02.045
53. P. Yadav, A. Kumar, A. Sanger, Y.K. Gautam, & B. P. Singh, *J. Electron. Mater.* **2021,** *50*, 192–200. **DOI:**10.1007/s11664-020-08588-8
54. N. Sarıca, O. Alev, L. Ç. Arslan, & Z. Z. Öztürk, *Thin Solid Films*. **2019,** *685*, 321–328. **DOI:**10.1016/j.tsf.2019.06.046
55. O. Şişman, N. Kılınç, & Z.Z. Öztürk, *Sens. Actuators, B.* **2016,** *236*, 1118–1125. **DOI:**10.1016/j.snb.2016.06.148
56. B. Biswas, A. Dey, S. Roy, S. Ray, & S. K. Sarkar, *IEEE.* **2019,** 202–205. **DOI:**10.1109/DEVIC.2019.8783477
57. N. Wu, M. Zhao, J. G. Zheng, C. Jiang, B. Myers, S. Li, & S. X. Mao, *Nanotechnology*. **2005,** *16*, 2878. **DOI:**10.1088/0957-4484/16/12/024
58. L. Presmanes, A. Chapelle, F. Oudrhiri-Hassani, A. Barnabé, & P.H. Tailhades, *Sens. Lett.* **2011,** *9*, 587–590. **DOI:**10.1166/sl.2011.1568
59. M. R. Yu, R. J. Wu, & M. Chavali, *Sens. Actuators, B*. **2011,** *153*, 321–328. **DOI:**10.1016/j.snb.2010.09.071

Povzetek

Z metodo elektropredenja (electrospinning) smo uspešno sintetizirali nanovlakna CuO. Nanodelce CuO smo preiskovali z namenom detekcije vodika in ogljikovega monoksida. Strukturne lastnosti sintetiziranih nanodelcev smo preučevali s Fourierjevo infrardečo spektroskopijo (FTIR), rentgensko difrakcijo (XRD), energijsko disperzivno rentgensko spektroskopijo (EDX) in morfologijo delcev z vrstično elektronsko mikroskopijo (SEM). Posnetki SEM so pokazali nanovlaknasto strukturo. Senzorji, zasnovani na nanodelcih CuO, so izkazali odlično sposobnost zaznavanja plinov pri temperaturi 175 °C in hiter odziv pri nizkih koncentracijah. Poleg tega smo opazili tudi dobro stabilnost, primerno ponovljivost in odlično selektivnost. Rezultati kažejo na možnost uporabe nanodelcev CuO pri detekciji H_2 (10–200 ppm) in CO (400–700ppm).